Ultrathin flexible dual band terahertz absorber

Yan Shan, Lin Chen *, Cheng Shi, Zhaoxiang Cheng, Xiaofei Zang, Boqing Xu, Yiming Zhu *

Shanghai Key Lab of Modern Optical System, Engineering Research Center of Optical Instrument and System, Ministry of Education, University of shanghai for Science and Technology, No. 516 JunGong Road, Shanghai 200093, China

ARTICLE INFO

ABSTRACT

We propose an ultrathin and flexible dual band absorber operated at terahertz frequencies based on metamaterial. The metamaterial structure consists of periodical split ring resonators with two asymmetric gaps and *a* metallic ground plane, separated by *a* thin-flexible dielectric spacer. Particularly, the dielectric spacer is *a* free-standing polyimide film with thickness of 25 μm, resulting in highly flexible for our absorber and making it promising for non-planar applications such as micro-bolometers and stealth aircraft. Experimental results show that the absorber has two resonant absorption frequencies (0.41 THz and 0.75 THz) with absorption rates 92.2% and 97.4%, respectively. The resonances at the absorption frequencies come from normal dipole resonance and high-order dipole resonance which is inaccessible in the symmetrical structure. Multiple reflection interference theory is used to analyze the mechanism of the absorber and the results are in good agreement with simulated and experimental results. Furthermore, the absorption properties are studied under various spacer thicknesses. This kind of metamaterial absorber is insensitive to polarization, has high absorption rates (over 90%) with wide incident angles range from 0° to 45° and the absorption rates are also above 90% when wrapping it to a curved surface.

© 2015 Elsevier B.V. All rights reserved.

1. Introduction

The electromagnetic (EM) metamaterials are a class of artificial structures with astonishing properties, such as negative refraction. Due to their unusual characteristics which cannot be found in nature materials, many research studies have been carried out in many applications, such as super lens [1], filters [2–4], waveguide [5], cloaking [6], absorbers [7–11], and so on. Since N. I. Landy firstly presented metamaterial absorber (MMA) with nearly unity absorptivity in 2008 [7], the perfect absorbers have attached great interests in recent years due to the potential applications to thermal emitter [12], bolometer [13] sensing [14], etc. Recently, perfect MMAs operated at various frequency spectra ranging from microwave through terahertz (THz) to optical band, which had been demonstrated by using different metamaterial resonators [15–18] and multilayer approaches [19,20]. In this paper, we propose *a* dual band and ultra-flexible THz absorber by using split ring resonators (SRRs) with two asymmetric gaps. Importantly, the majority of previous THz absorbers are patterned on rigid substrates, such as silicon, which are limited for applications on curved surfaces [21–23]. However our designed structure is on *a* highly flexible polyimide (PI) film with thickness of 25 μm without a rigid substrate, and can easily be wrapped into cylinder with a radius of *a* few

millimeters. As it is flexible, low cost and conformable adhesion, the absorber can be used in non-planar or conformal geometry applications such as covering the fuselage of stealth aircraft or being applied in micro-bolometers to absorb radiant power at certain frequencies [24,25]. The metamaterial based on SRR with broken symmetry had been widely studied to achieve electromagnetic induced transparency (EIT) effect or Fano resonance [26–29], but few research applied this structure to absorber applications. In our work, we experimentally find the absorber shows two distinctive absorption peaks at frequencies of 0.41 THz and 0.75 THz with absorption rates 92.2% and 97.4%, respectively. Comparing the properties of symmetric structure to that of asymmetric structure, a high-order dipole resonance exists in the later one. The resonance mode in asymmetric structure arises from the coupling between horizontal and vertical arms. We employ multi-reflection interference theory model [30,31] to investigate the mechanism of this absorber and verify the validity of theoretical calculation by comparing with numerical simulated and experimental results. The influence of the spacer thickness is discussed to further understand magnitude and phase conditions of the theory. Also, the absorber is studied under different polarization angles and various incident angles in order to prove the designed structure is omnidirectional and polarization-insensitive for both TE and TM polarization. In addition, the absorption properties with curved surface are researched, which exhibit high absorption rates (over 90%). Our flexible absorber enables many promising applications in THz field such as antennas, filtering and stealth technologies.

* Corresponding authors. Fax: +86 21 33773176.
  E-mail addresses: linchen@usst.edu.cn (L. Chen), ymzhu@usst.edu.cn (Y. Zhu).

2. Design and experiment

The unit cell of the designed polarization-independent MMA consists of 2 × 2 array of SRRs, in which the single SRR "2" is in 90° rotation with SRR "1". SRRs "1" and "3" have the same directions and SRRs "2" and "4" have the same directions, as shown in Fig. 1(a). The complete MMA is the periodic extension of the unit cell in both "*x*" and "*y*" directions, as given in Fig. 1(c). All four SRRs in the unit cell have the same dimensions with the single SRR illustrated in Fig. 1(b), and the final optimized geometrical parameters are as follows: $a = 153$ μm, $l = 131$ μm, $w = 8$ μm, and $g = 10$ μm. The fabricated sample contains three layers: the top layer is an array of aluminum (Al) patterns which were 0.2 μm-thick and were fabricated by conventional optical lithography, the lower layer is a 0.2 μm-thick Al film without any structure. This Al plate is magnetron sputtered to totally eliminate the transmission of the structure across the entire frequency range. So the absorption is calculated by $A(w) = 1 - R(w) - T(w) = 1 - |S_{11}|^2 - |S_{21}|^2 = 1 - |S_{11}|^2$. Between the two metallic layers, a 25 μm-thick polyimide film is used as dielectric spacer to separate them. Due to the low thickness of the polyimide, the absorber has good mechanical flexibility (see Fig. 1 (d)), which is suitable for widely used in THz field.

The numerical simulation of the designed MMA was carried out by using commercial software, CST Microwave Studio. The wave propagation direction is perpendicular to the plane of the SRRs array and electric field polarized perpendicular to the gaps at normal incidence. Both Al layers were modeled as lossy metal with electrical conductivity of $\sigma = 3.56 \times 10^7$ s/m (behave almost like perfect conductor compared to visible region [32]), and the
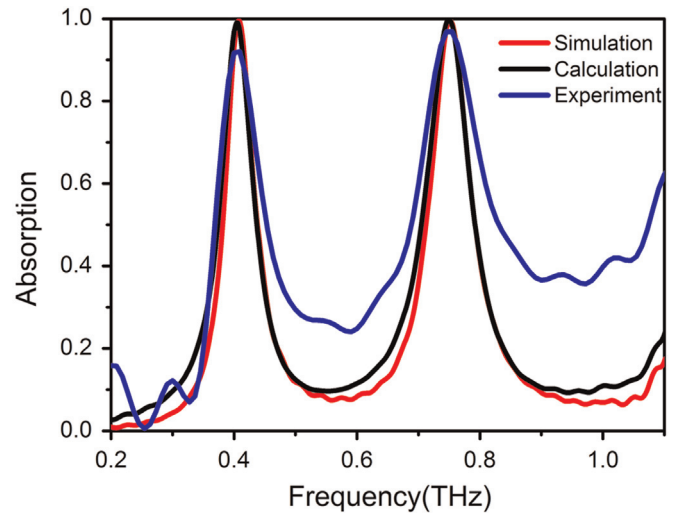
Fig. 2. The comparison of absorption spectrum among simulation (red line), experiment (blue line) and theoretical calculation (dark line). (For interpretation of the references to color in this figure legend, the reader is referred to the web version of this article.)

polyimide spacer is taken as a lossy material with dielectric constant of $\varepsilon = 3.4$ and dielectric loss tangent of $\tan(\delta) = 0.09$. The simulated absorption is shown in Fig. 2 (red line), revealing two absorption peaks at the frequencies 0.41 THz and 0.75 THz with absorption rates 99.7% and 99.6%, respectively. In the experiment, the total size of our sample is 15 mm × 15 mm. Furthermore the
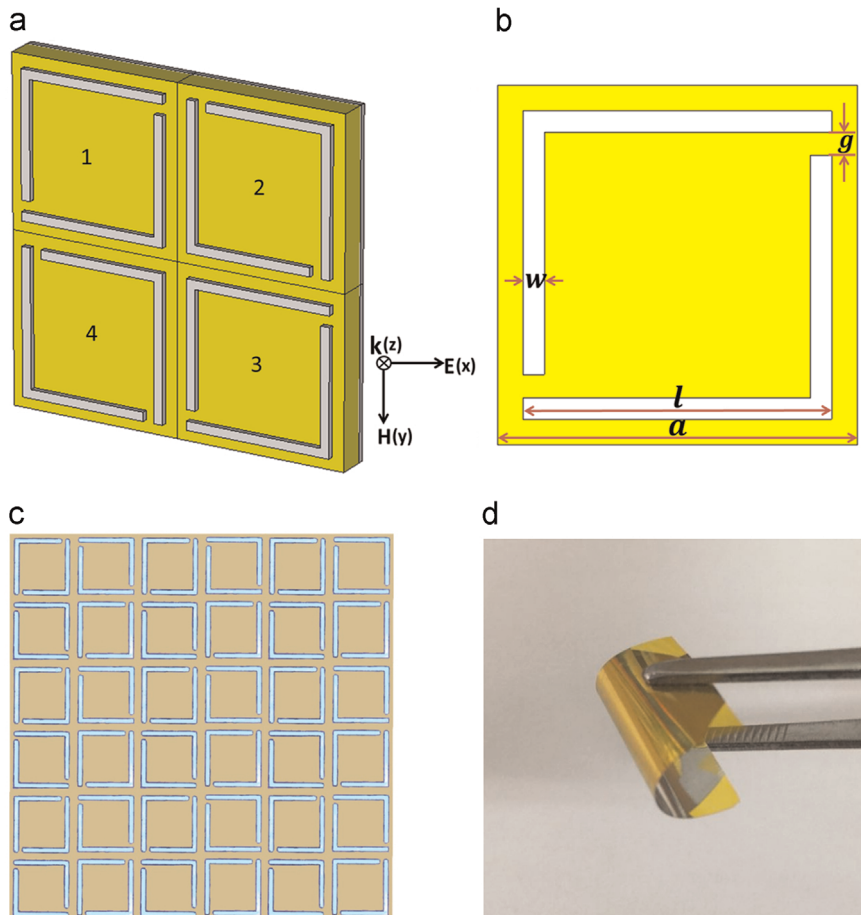
Fig. 1. The schematic of dual band absorber. (a) The perspective view of unit cell. (b) The front view of the single SRR. (c) The fabricated structure and (d) the photograph of thin-flexible dielectric spacer with a layer of Al film.

reflection spectra S_{11} was measured by applying fast and slow scan-based THz time domain spectroscopy (THz-TDS) and a smooth and unpatterned metallic mirror is used as reference when testing reflection [33–35]. As shown in Fig. 2, the measurement result (black line) demonstrates that the absorption rates can reach 92.2% and 97.4% at frequencies of 0.41 THz and 0.75 THz, respectively, which has slight difference with the simulation result. The difference is caused by fabrication and measurement tolerances.

To verify the resonance mechanism at the frequencies of two absorption peaks, we simulated the changing progresses that two gaps of the single SRR change from symmetry to asymmetry shown in Fig. 3. Only one absorption peak can be excited when the SRR is perfectly symmetric with the two gaps being placed exactly along the central horizontal axis, as shown in Fig. 3(a). As soon as asymmetry in the SRR is introduced by simultaneously displacing the two gaps from its center towards opposite corners by displacement distance "d", as shown in Fig. 3(b), another new absorption peak can be observed at a different frequency around 0.75 THz (Fig. 3(d)). With the increasing of gaps displacement (Fig. 3(c)), the resonance intensity at the high-frequency absorption peak becomes stronger, and resulting in a gradually enhanced absorption. As the SRR gaps are pushed to extreme corner (i.e.d=51.5 μm), the absorption around 0.75 THz changes from 0% to 93.9%, the low-frequency peak blue shift by 0.03 THz and high-frequency peak red shift by 0.04 THz.

To understand the underlying resonance mechanism, the electric field and surface currents distributions of the absolutely symmetric structure ($d = 0$ μm) and extreme asymmetric structure ($d = 51.5$ μm) are depicted in Fig. 4. For the symmetric structure, the absorption peak (0.35 THz) is evoked by the in-phase dipole resonances along the two horizontal arms, as shown in Fig. 4 (a) and (d). As the symmetry is broken, the low-frequency resonance mode (0.38 THz) is similar to the dipole resonance of

symmetric structure, and two in-phase dipole modes are excited by two half rings of SRRs, as shown in Fig. 4(b) and (e). However, two high-order dipole modes are observed at the high-frequency absorption peak (0.75 THz), as shown in Fig. 4(c) and (f). The surface currents of the upper ring diverge from corner to two arms, and the currents of the lower ring converge to the corner from two arms. This is because the two horizontal bars are directly excited by the incident THz wave. Then, they couple to the vertical bars to excite an additional dipole mode [36]. As a consequence, two opposite charges accumulate in the facing edges resemble classical capacitance. The resonance property is inaccessible in the symmetrical structure. When the SRR gaps are displaced from symmetric to extreme asymmetric position, the absorption frequencies have slightly shift because the alterations in nearby vertical SRR arms modify the radiation properties of the dipole oscillating along the incident electric field direction [27].

3. The interference theory

The physical mechanism of our proposed dual band absorber is further elucidated in this part. Initially, the idea is that the unity absorption comes from impedance matching [8]. It is complained as the reflection will be minimized when the effective impedance of MMA (defined as $Z(w) = \sqrt{\mu(w)/\varepsilon(w)}$) matches to the free space impedance Z_0 at certain frequencies. However, recent research shows that the high absorption originated from destructive interference of multi-reflection, and there is no magnetic response between the top and bottom metal structures or the magnetic response is weak to be neglected [23,37,38]. Here we adopt multiple reflections interference model [30,31] to analyze the performance of reflection quantitatively which cannot be realized using impedance matching theory.
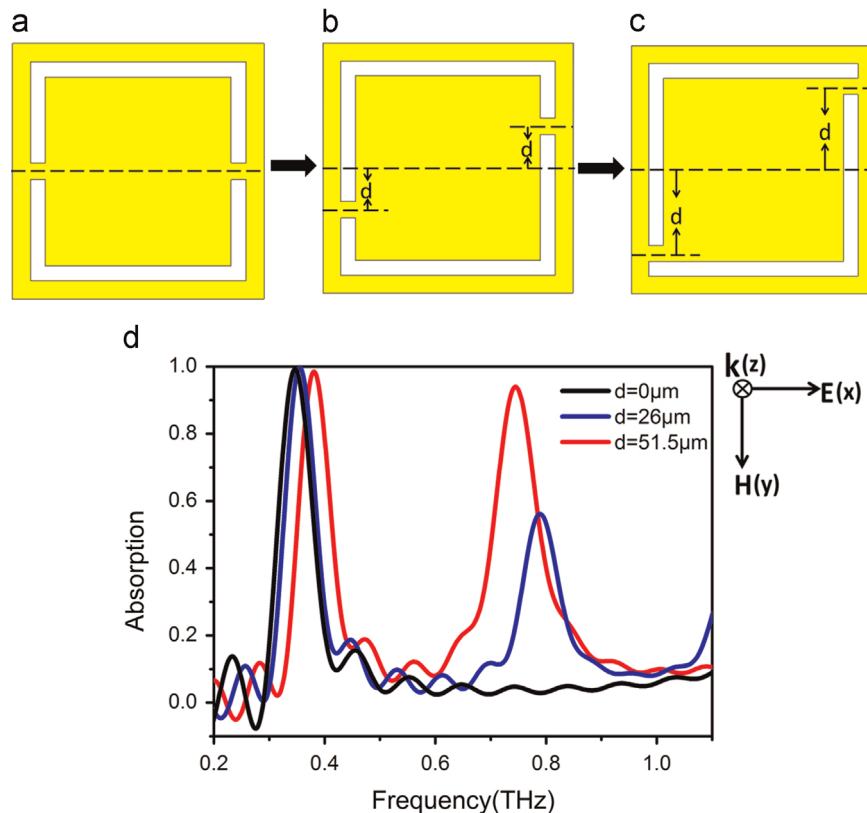
Fig. 3. The structures of different distance (a) d=0 μm, (b) d=26 μm and (c) d=51.5 μm. (d) Simulated absorption spectra of three different structures with d=0 μm (dark line), d=26 μm (blue line), d=51.5 μm (red line). (For interpretation of the references to color in this figure legend, the reader is referred to the web version of this article.)
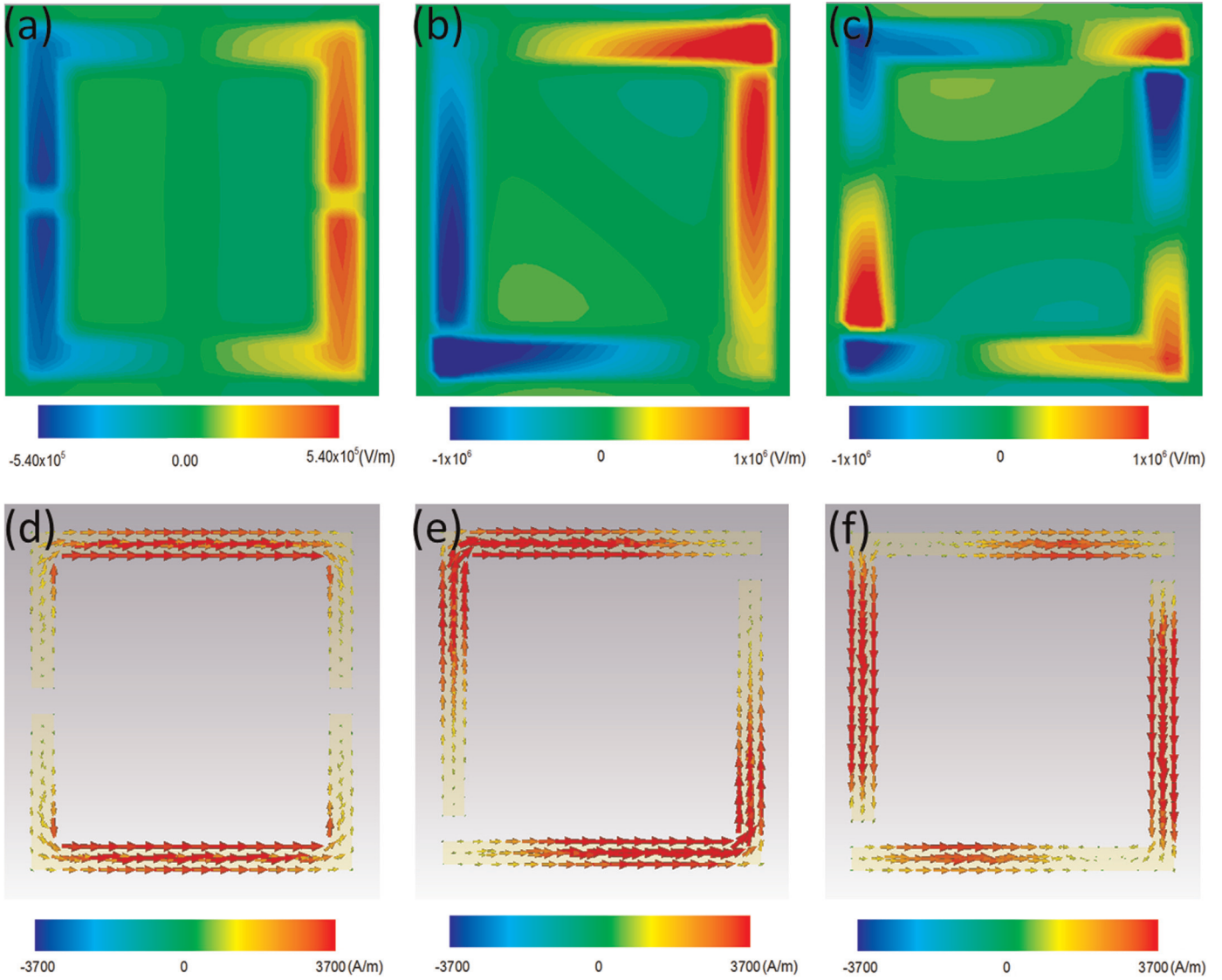
Fig. 4. (a) Electric fields and (d) surface current distributions at 0.35 THz (the absorption peak) when $d = 0$ μm, (b) electric fields and (e) surface current distributions at 0.38 THz (low-frequency absorption peak) when $d = 51.5$ μm, (c) electric fields and (f) surface current distributions at 0.75 THz (high-frequency absorption peak) when $d = 51.5$ μm.

As depicted in Fig. 5(a), the model contains two interfaces: the air-spacer with SRR array and spacer-substrate. The top Al pattern and ground plane are simplified with zero thickness. When a plane wave is incident upon the air-spacer interface, a part of the incident light is reflected back to air with the reflection coefficient $\tilde{r}_{12} = r_{12}e^{i\varnothing_{12}}$, the other part transmits into spacer layer with the transmission coefficient $\tilde{t}_{12} = t_{12}e^{i\theta_{12}}$. The latter part continues to propagate in polyimide until it reaches the bottom metal layer and is totally reflected with reflection coefficient $\tilde{r}_{23} = -1 = e^{i\pi}$. Partial reflection and transmission occur again when the above light is incident to air-spacer interface with coefficients $\tilde{r}_{21} = r_{21}e^{i\varnothing_{21}}$ and $\tilde{t}_{21} = t_{21}e^{i\theta_{21}}$. The process of multiple reflections is illustrated in Fig. 5. According to the interference theory, the overall reflected wave from air-spacer interface is superposition as:

$$\tilde{r} = \tilde{r}_{12} + \frac{\tilde{t}_{12}\tilde{t}_{21}e^{i(\pi+2\tilde{\beta})}}{1 - \tilde{r}_{21}e^{i(\pi+2\tilde{\beta})}} = \frac{\tilde{r}_{12} - (\tilde{r}_{12}\tilde{r}_{21} - \tilde{t}_{12}\tilde{t}_{21})e^{i(\pi+2\tilde{\beta})}}{1 - r_{21}e^{i(\varnothing_{21}+\pi+2\tilde{\beta})}} \quad (1)$$

Here $\tilde{\beta} = -\sqrt{\varepsilon_{\text{spacer}}}k_0 t$ is complex propagation phase, k_0 is the wavenumber in free space and t is the thickness of spacer.

The magnitude and phase coefficients at two interfaces are

obtained by using CST software, as shown in Figs. 5(c) and 5(d). The reflection spectra can be calculated through Eq. (1). Fig. 5 (b) shows the calculated reflectance and absorption spectrum, which is in excellent agreement with numerical simulation. It is observed from Fig. 5 and Eq. (1), only when the conditions (i) $|\tilde{r}_{12}| - |\tilde{r}_{12}\tilde{r}_{21} - \tilde{t}_{12}\tilde{t}_{21}| \approx 0$ and (ii) $\varnothing_{21} + \pi + 2\beta \approx 2m\pi$ (here m represents integer) are satisfied at the same frequencies simultaneously, could the destructive interference occur among multiple reflections and the reflection be nearly zero. Therefore perfect absorber with nearly unity absorption is realized, which had been discussed in [30] and [31]. In Fig. 5(c), we use parameter "rt" to represent the magnitude of $\tilde{r}_{12}\tilde{r}_{21} - \tilde{t}_{12}\tilde{t}_{21}$, i.e., $rt = |\tilde{r}_{12}\tilde{r}_{21} - \tilde{t}_{12}\tilde{t}_{21}|$.
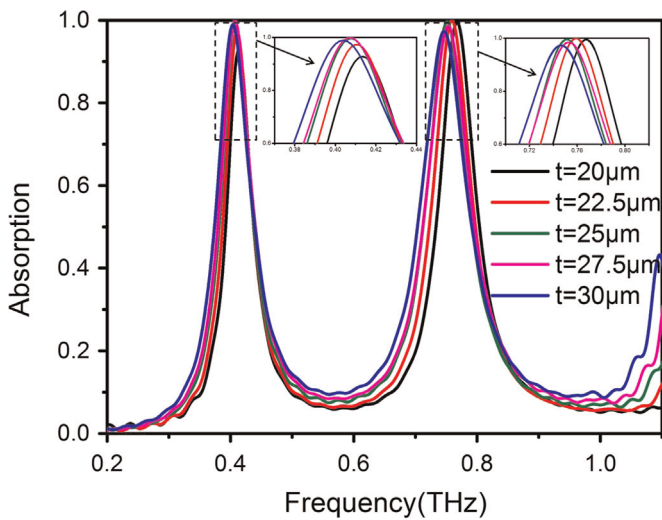
4. Analysis and discussion

4.1. Absorption properties with different spacer thicknesses

The simulated results are carried out on a series of spacer thickness t to characterize the absorption properties of the MMA, as shown in Fig.6. As the spacer thickness t increases from 20 μm
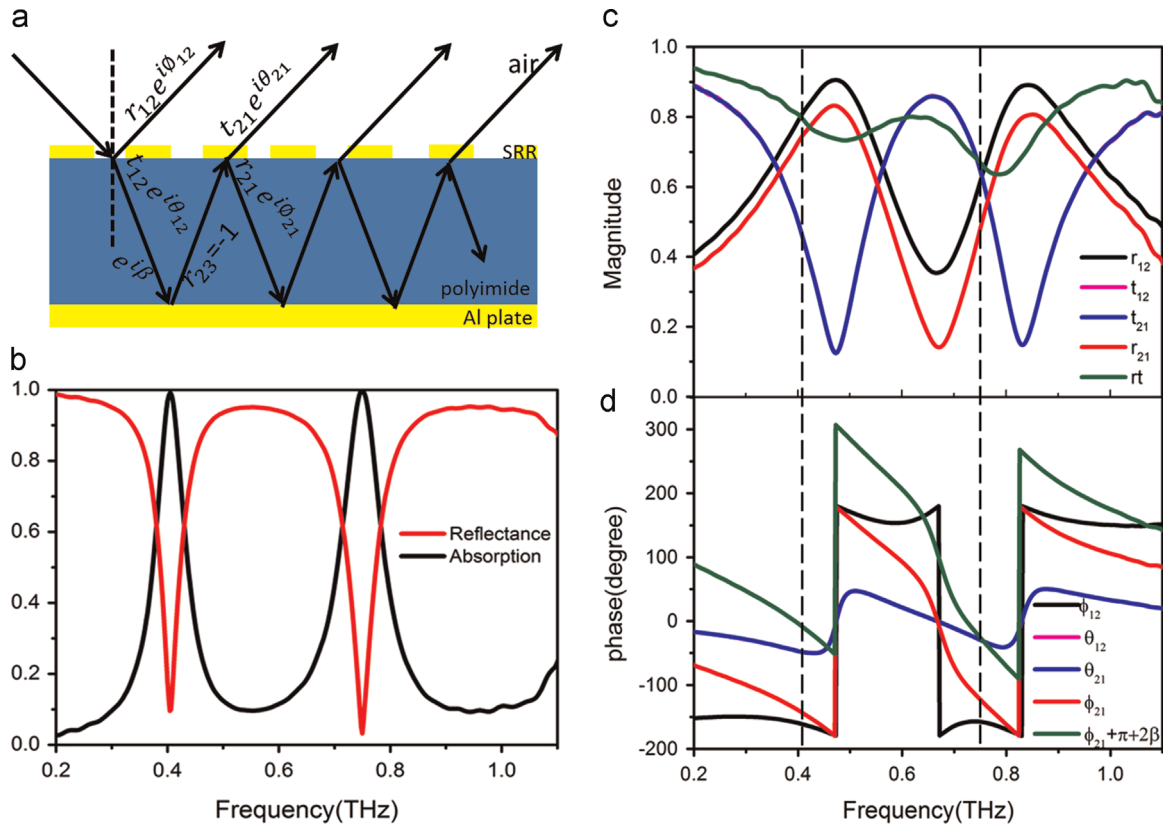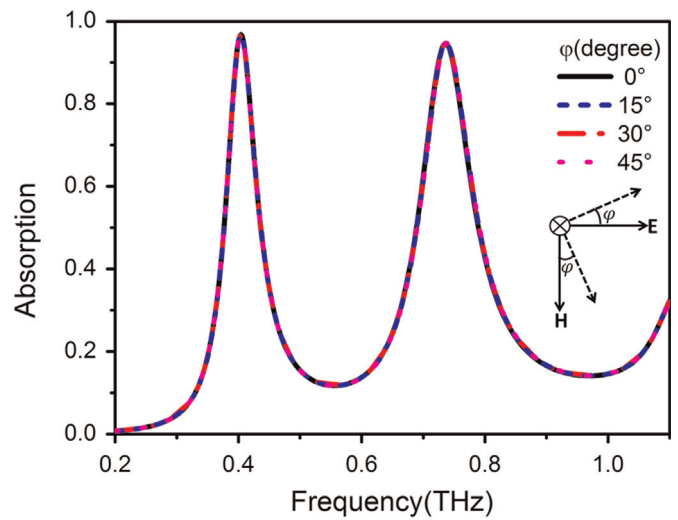
Fig. 5. (a) Illustration of multiple reflections interference model of the metamaterial absorber. (b) The calculated reflectance (red line) and absorption rate (black line). (c) The magnitude and (d) phase of the complex reflection and transmission coefficients at interfaces. The vertical dashed lines in (c) and (d) indicate the absorption frequencies. (For interpretation of the references to color in this figure legend, the reader is referred to the web version of this article.)

Fig. 6. The absorptions for various spacer thicknesses. Insets: two enlarged absorption peaks.

Fig. 7. Simulated absorptions under normal incident EM wave with different polarization angles.

to 25 μm, the absorption rates of two peaks increase and their frequencies red shift slightly. It reaches near-unity absorption for 0.41 THz and 0.75 THz simultaneously when the thickness is about 25 μm. As the thickness t increases further, the absorption values gradually decrease and the frequencies keep red shift. This is because when the spacer thickness deviates from the optimized value (i.e. $t = 25$ μm), the magnitude and phase conditions cannot match any more and the multiple reflections partially interfere destructively or may add each other constructively. So the corresponding frequencies of absorption peaks shift when the spacer

thickness changes from 20 μm to 30 μm, and the absorption rates reduce when the frequencies go away from the center frequencies (i.e. 0.41 THz and 0.75 THz).

4.2. Absorption properties with different polarization angles

Here, we study the performance of the absorber under different angles (φ) of polarization, as shown in Fig. 7. Since the unit cell of the MMA is formed with 2×2 array of SRRs oriented in different directions, the structure is studied at various angles of polarization
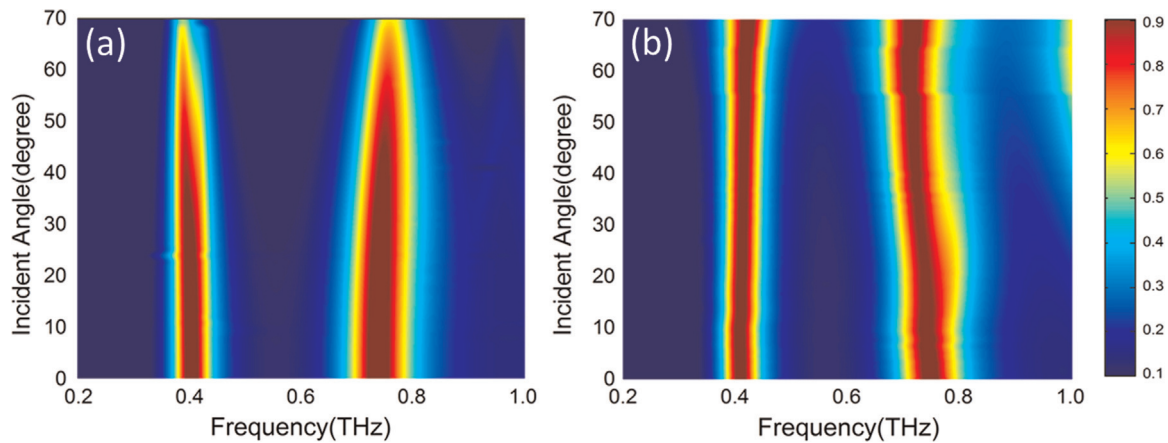
Fig. 8. The simulated absorptions at various incident angles for (a) TE and (b) TM polarization.

only from 0° to 45°. In all these cases, the incident THz wave is normal incidence. From Fig. 7, it is observed that at all cases of polarization angle, the absorption rates are nearly the same. The results indicate that the proposed structure is an insensitive-polarization absorber.

4.3. Absorption properties with different incident angles

For practical application, we also evaluate the absorber at different angles of incidence for TE and TM polarization. The simulated absorption rates as a function of frequency and incident angle are illustrated in Fig. 8. For TE polarization, the absorption rates are all remain above 90% when the angle of incidence changes from 0° to 45°. As the angle of incidence is larger than 45°, the absorption rates of both peaks gradually decrease. This may be explained that at larger angles of incidence the effective electric field is less than the case of normal incidence, therefore, the overall absorption is weakened for the magnitude and phase conditions cannot be satisfied any more. For TM wave, the absorption rate is hardly influenced by increasing incident angle, only the high absorption frequency has little red shift. Both of the absorption peaks are larger than 95%, since the reflection and
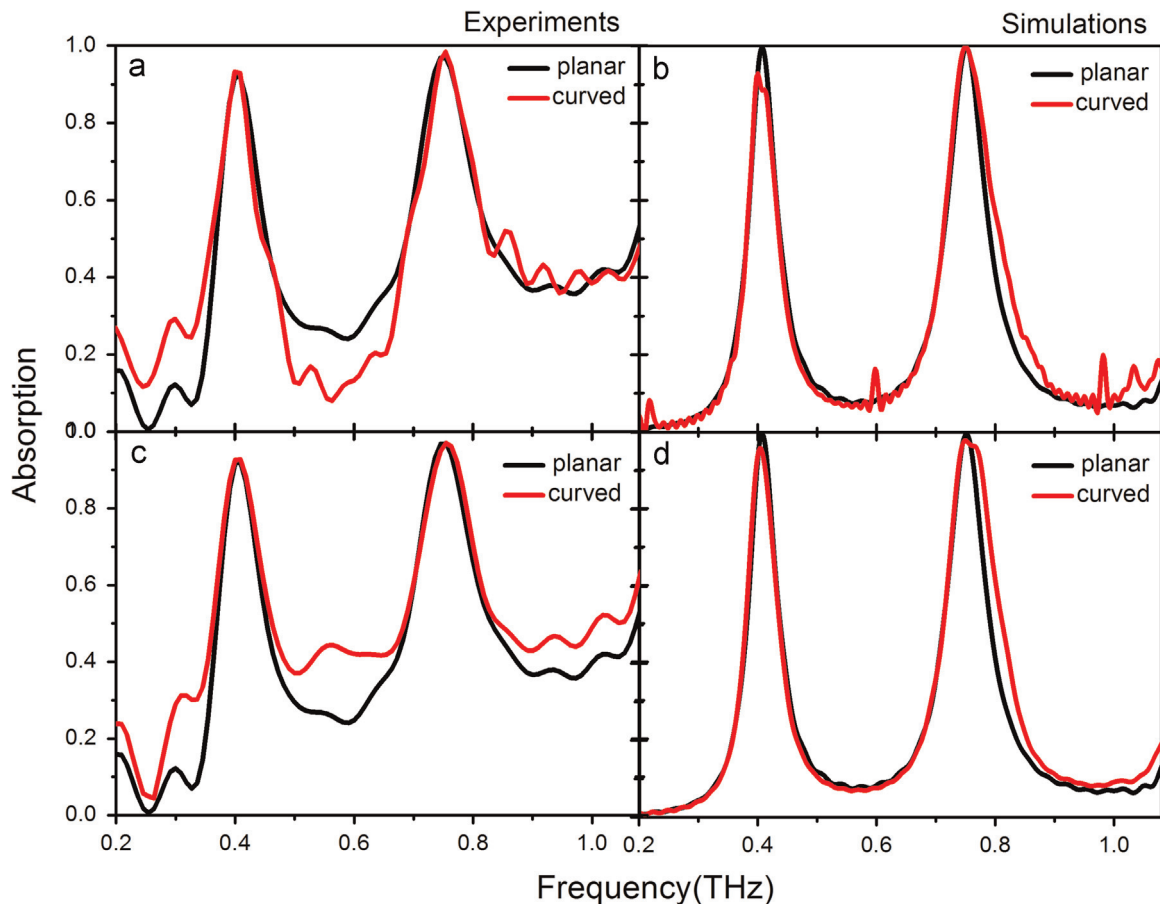

Fig. 9. (a) Measured and (b) simulated absorption of planar absorber (black line) and curved absorber (red line) for TE polarization, (c) measured and (d) simulated absorption of planar absorber (black line) and curved absorber (red line) for TM polarization. (For interpretation of the references to color in this figure legend, the reader is referred tothe web version of this article.)

transmission coefficients at two interfaces are less sensitive to incident angle. These simulated results indicate that the proposed absorber can behave well for obliquely incident wave.

4.4. Absorption properties with curved structure

We have wrapped our absorber around a cylinder with radius of approximately 5.5 mm to form a curved surface. The measurements of the absorption for both TE polarization and TM polarization indicate a neglected difference between planar structure (black line) and curved surface (red line), as shown in Fig.9(a) and (c). Fig.9(b) and (d) are the simulated results, which are in good agreement with the measured results. In the curved surface, different unit cells experience different incident angles, normal incidence only occurs on the center of the absorber, the other areas experience oblique incidence. In addition, the absorption rates of our absorber can remain above 90% with incident angles range from 0° to 45° for TE polarization and remain above 95% with all incidence angles for TM polarization, which has been detailed analyzed above. Therefore, the absorption rates are over 90% for most unit cells of the curved absorber. These results suggest that such absorber is suitable for a curved surface.

5. Conclusion

In summary, we have proposed an ultrathin flexible dual band THz absorber based on square SRRs with two asymmetric gaps, which works at 0.41 THz and 0.75 THz. At the low-frequency absorption peak, the resonance is a dipole mode, however, a high-order dipole mode is observed at the high-frequency absorption peak, which is inaccessible in the symmetrical structure. Multiple reflections interference model is used to quantitatively explain the physical mechanism of the MMA. The theoretical calculations, experimental results and numerical simulations are in excellent agreement. Furthermore, the omnidirectional and polarization-insensitive property with both TE and TM polarization are demonstrated for the designed MMA. And the good absorption performance on a curved surface indicates the proposed absorber is suitable for many non-planar and conformal geometry applications in THz field.

References

[1] N. Fang, H. Lee, C. Sun, X. Zhang, Sub-diffraction-limited optical imaging with a silver superlens, Science 308 (2005) 534.
[2] L. Chen, Y.M. Zhu, X.F. Zang, B. Cai, Z. Li, L. Xie, S.L. Zhuang, Mode splitting transmission effect of surface wave excitation through a metal hole array, Light Sci. Appl. 2 (2013) e60.
[3] L. Chen, K.V. Truong, Z.X. Cheng, Z. Li, Y.M. Zhu, Characterization of photonic bands in metal photonic crystal slabs, Opt. Commun. 333 (2014) 232–236.
[4] Z.X. Cheng, L. Chen, X.F. Zang, B. Cai, Y. Peng, Y.M. Zhu, Ultrathin dual-mode filtering characteristics of terahertz metamaterials with electrically unconnected and connected U-shaped resonators array, Opt. Commun. 342 (2015) 20–25.
[5] K. Yamamoto, S. Nomura, Energy compensated mode in a waveguide composed of lossy left-handed metamaterial, Opt. Commun. 276 (2007) 191.
[6] D. Schurig, J.J. Mock, B.J. Justice, S.A. Cummer, J.B. Pendry, A.F. Starr, D.R. Smith, Metamaterial electromagnetic cloak at microwave frequencies, Science 314 (2006) 977.
[7] N.I. Landy, S. Sajuyigbe, J.J. Mock, D.R. Smith, W.J. Padilla, A perfect metamaterial absorber, Phys. Rev. Lett. 100 (2008) 207402.
[8] L. Li, Y. Yang, C.H. Liang, A wide-angle polarization-insensitive ultra-thin metamaterial absorber with three resonant modes, J. Appl. Phys. 110 (2011) 063702.
[9] H. Tao, N.I. Landy, C.M. Bingham, X. Zhang, R.D. Averitt, W.J. Padilla, A metamaterial absorber for the terahertz regime: design, fabrication and characterization, Opt. Express 16 (2008) 7181.
[10] G.H. Li, X.S. Chen, O.P. Li, C.X. Shao, Y. Jiang, L.J. Huang, B. Ni, W.D. Hu, W. Lu, A novel plasmonic resonance sensor based on an infrared perfect absorber, J. Phys. D: Appl. Phys. 45 (2012) 205102.
[11] X.P. Shen, C.T. Jun, Y.J. Xiang, Dual band metamaterial absorber in microwave regime, Acta Phys. Sin. 61 (2012) 058101.
[12] X.L. Liu, T. Tyler, T. Starr, A.F. Starr, N.M. Jokerst, W.J. Padilla, Taming the blackbody with infrared metamaterials as selective thermal emitters, Phys. Rev. Lett. 107 (2011) 045901.
[13] F.B.P. Niesler, J.K. Gansel, S. Fischbach, M. Wegener, Metamaterial metal-based bolometers, Appl. Phys. Lett. 100 (2012) 203508.
[14] C. Sabah, F. Dincer, M. Karaaslan, E. Unal, O. Akgol, E. Demirel, Perfect metamaterial absorber with polarization and incident angle independencies based on ring and cross-wire resonators for shielding and a sensor application, Opt. Commun. 322 (2014) 137.
[15] Y.J. Huang, Y.R. Tian, G.J. Wen, W.R. Zhu, Experimental study of absorption band controllable planar metamaterial absorber using asymmetrical snow-flake-shaped configuration, J. Opt. 15 (2013) 055104.
[16] Y. Ma, Q. Chen, J. Grant, S.C. Saha, A. Khalid, D.R.S. Cumming, A terahertz polarization insensitive dual band metamaterial absorber, Opt. Lett. 36 (2011) 945.
[17] K.B. Alici, A.B. Turhan, C.M. Soukoulis, E. Ozbay, Optically thin composite resonant absorber at the near-infrared band: a polarization independent and spectrally broadband configuration, Opt. Express 19 (2011) 14260.
[18] S. Bhattacharyya, K.V. Srivastava, Triple band polarization-independent ultra-thin metamaterial absorber using electric field-driven LC resonator, J. Appl. Phys. 115 (2014) 064508.
[19] H. Luo, X.H. Hu, Y. Qiu, P. Zhou, Design of a wide-band nearly perfect absorber based on multi-resonance with square patch, Solid State Commun. 188 (2014) 5.
[20] J. Wu, C.H. Zhou, J.J. Yu, H.C. Cao, S.B. Li, W. Jia, TE polarization selective absorber based on metal-dielectric grating structure for infrared frequencies, Opt. Commun. 329 (2014) 38.
[21] H. Tao, C.M. Bingham, D. Pilon, K. Fan, A.C. Strikwerda, D. Shrekenhamer, W. J. Padilla, X. Zhang, R.D. Averitt, A dual band terahertz metamaterial absorber, J. Phys. D: Appl. Phys. 43 (2010) 225102.
[22] Q.Y. Wen, H.W. zhang, Y.S. Xie, Q.H. Yang, Y.L. Liu, Dual band terahertz metamaterial absorber: design, fabrication, and characterization, Appl. Phys. Lett. 95 (2009) 241111.
[23] P.V. Tuong, J.W. Park, J.Y. Rhee, K.W. Kim, W.H. Jang, H. Cheong, Y.P. Lee, Polarization-insensitive and polarization-controlled dual-band absorption in metamaterials, Appl. Phys. Lett. 102 (2013) 081122.
[24] K. Fan, X. Zhao, J. Zhang, K. Geng, G.R. Keiser, H.R. Seren, G.D. Metcalfe, M. Wraback, X. Zhang., R.D. Averitt, Optically tunable terahertz metamaterial on highly flexible substrates, IEEE Trans. Terahertz Sci. Technol. 3 (2013) 702.
[25] H. Tao, C.M. Bingham, A.C. Strikwerda, D. Pilon, D. Shrekenhamer, N.I. Landy, K. Fan, X. Zhang, W.J. Padilla, R.D. Averitt, Highly flexible wide angle of incidence terahertz metamaterial absorber: design, fabrication, and characterization, Phys. Rev. B 78 (2008) 241103.
[26] R. Singh, I.A.I. Al-Naib, Y. Yang, D.R. Chowdhury, W. Cao, C. Rockstuhl, T. Ozaki, R. Morandotti, W. Zhang, Observing metamaterial induced transparency in individual Fano resonators with broken symmetry, Appl. Phys. Lett. 99 (2011) 201107.
[27] R. Singh, I.A.I. Al-Naib, M. Koch, W. Zhang, Asymmetric planar terahertz metamaterials, Opt. Express 18 (2010) 13044.
[28] J.H. Shi, Z. Zhu, H.F. Ma, W.X. Jiang, T.J. Cui, Tunable symmetric and asymmetric resonances in an asymmetrical split-ring metamaterial, J. Appl. Phys. 112 (2012) 073522.
[29] R. Singh, I.A.I. Al-Naib, M. Koch, W. Zhang, Sharp Fano resonances in THz metamaterials, Opt. Express 19 (2011) 6312.
[30] H.-T. Chen, J. Zhou, J.F. O'Hara, F. Chen, A.K. Azad, A.J. Taylor, Antireflection coating using metamaterials and identification of its mechanism, Phys. Rev. Lett. 105 (2010) 073901.
[31] H.-T. Chen, Interference theory of metamaterial perfect absorbers, Opt. Express 20 (2012) 7165.
[32] L. Chen, Z.Q. Cao, F. Ou, H.G. Li, Q.S. Shen, H.C. Qiao, Observation of large positive and negative lateral shifts of a reflected beam from symmetrical metal-cladding waveguides, Opt. Lett. 32 (2007) 1432–1434.
[33] L. Chen, C.M. Gao, J.M. Xu, X.F. Zang, B. Cai, Y.M. Zhu, Observation of

electromagnetically induced transparency-like transmission in terahertz asymmetric waveguide-cavities systems, Opt. Lett. 38 (2013) 1379–1381.

[34] L. Chen, J.M. Xu, C.M. Gao, X.F. Zang, B. Cai, Y.M. Zhu, Manipulating terahertz electromagnetic induced transparency through parallel plate waveguide cavities, Appl. Phys. Lett. 103 (2013) 251105.

[35] L. Chen, Z.X. Cheng, J.M. Xu, X.F. Zang, B. Cai, Y.M. Zhu, Controllable multiband terahertz notch filter based on a parallel plate waveguide with a single deep groove, Opt. Lett. 39 (2014) 4541–4544.

[36] J.F. Liu, Q.L. Zhou, Y.L. Shi, X. Zhao, C.L. Zhang, Study of L-shaped resonators at terahertz frequencies, Appl. Phys. Lett. 103 (2013) 241911.

[37] J. Wang, Y. Chen, J. Hao, M. Yan, M. Qiu, Shape-dependent absorption characteristics of three-layered metamaterial absorbers at near-infrared, J. Appl. Phys. 109 (2011) 074510.

[38] C.H. Wu, B. Neuner, G. Shvets, J. John, A. Milder, B. Zollars, S. Savoy, Large-area wide-angle spectrally selective plasmonic absorber, Phys. Rev. B 84 (2011) 075102.